SURFACE CHEMISTRY

Superaerophobic hydrogels for enhanced electrochemical and photoelectrochemical hydrogen production

Dasom Jeon[1,2]*, Jinwoo Park[3]*, Changhwan Shin[2,3], Hyunwoo Kim[1,2], Ji-Wook Jang[2,3], Dong Woog Lee[3]†, Jungki Ryu[1,2]†

The efficient removal of gas bubbles in (photo)electrochemical gas evolution reactions is an important but underexplored issue. Conventionally, researchers have attempted to impart bubble-repellent properties (so-called superaerophobicity) to electrodes by controlling their microstructures. However, conventional approaches have limitations, as they are material specific, difficult to scale up, possibly detrimental to the electrodes' catalytic activity and stability, and incompatible with photoelectrochemical applications. To address these issues, we report a simple strategy for the realization of superaerophobic (photo)electrodes via the deposition of hydrogels on a desired electrode surface. For a proof-of-concept demonstration, we deposited a transparent hydrogel assembled from M13 virus onto (photo)electrodes for a hydrogen evolution reaction. The hydrogel overlayer facilitated the elimination of hydrogen bubbles and substantially improved the (photo)electrodes' performances by maintaining high catalytic activity and minimizing the concentration overpotential. This study can contribute to the practical application of various types of (photo)electrochemical gas evolution reactions.

INTRODUCTION

Electrochemical and photoelectrochemical gas evolution reactions are not only academically interesting but also practically very important for the sustainable production and use of chemicals (*1*–*6*). Representative examples include the hydrogen and oxygen evolution reactions (HER and OER, respectively), which can be used to produce high-purity hydrogen fuels under mild conditions (e.g., ambient pressure and temperature) (*7*–*14*). These reactions are unique in that the three-phase interface of gas, liquid, and solid is formed by the evolved gases (*15*). The gas bubbles can be attached to electrodes and lower the efficiency of gas evolution reactions by (i) decreasing specific catalytic activity due to the blocking of active sites and (ii) increasing the concentration overpotential due to inefficient mass transport. However, researchers have paid relatively little attention to these issues, even though they have conducted numerous studies on the development of the HER and OER catalysts (*16*–*21*). Recently, researchers have found that surfaces with hierarchical nano- and microstructures can exhibit superaerophobicity (i.e., extreme bubble repellency) with an air-contact angle of greater than 150° and an air-sliding angle of less than 10° (*22*–*24*). Lu *et al.* (*25*) first reported the development of superaerophobic electrodes and found that MoS_2—a known HER catalyst—can easily eliminate hydrogen bubbles and has a higher electrochemical activity in the porous thin-film structure than in the flat counterpart. Thus far, researchers have used the nano- and microfabrication approaches to impart superaerophobicity for a limited number of materials, such as Pt nanoarrays for HER (*26*), NiFe-layered double hydroxides for OER (*27*), Cu_3P microsheets for overall water splitting (*28*), and RuO_2@TiO_2 nanosheet arrays for chlorine evolution reactions (*29*).

However, these approaches are not yet efficient enough to be used in practical applications due to fabrication difficulties and stability issues. These approaches are also difficult to scale up because they generally rely on harsh and complex processing conditions (high temperature and pressure, energy- and labor-intensive processes, etc.). In addition, these approaches are materials specific and thus are not universally applicable; only a few materials have been used for superaerophobicity, as described above. Furthermore, these approaches can hardly be used for photoelectrochemical applications because nano- and microstructures severely scatter light and have low light transmittance; that is evidenced by the lack of studies on superaerophobic photoelectrodes.

To address these issues, we report a new strategy for the fabrication of superaerophobic surfaces—particularly for (photo)electrochemical gas evolution reactions—in which a porous hydrogel overlayer is deposited on a target substrate. For the model system, under the hydrogel overlayer, we used Pt electrodes for electrochemical HER and Si photocathodes for photoelectrochemical HER. The hydrogel overlayer was readily prepared by cross-linking nanofibrillar M13 bacteriophages under mild conditions. This approach led to efficient HER due to the hydrogel's large surface area and high porosity, as well as its ability to separate the catalytically active and superaerophobic sites. Thus, hydrogen was readily produced on the underlying electrodes' surface by maintaining the high catalytic activity but was then eliminated through the highly porous superaerophobic hydrogel. For example, at 10 mA cm^{-2}, the hydrogel-coated Pt electrodes exhibited a substantially lower overpotential than the pristine ones (a difference of about 100 mV). The hydrogel remained stable for at least 30 hours without a noticeable degradation of the performance. The beneficial effect of the superaerophobic hydrogel was more pronounced at higher current densities. In addition, this approach can be used in photoelectrochemical gas evolution reactions because the hydrogel is transparent. In short, this study describes a new means of achieving efficient gas release reactions and provides academic insight into the design of novel (photo)electrochemical devices.

[1]Department of Energy Engineering, School of Energy and Chemical Engineering, Ulsan National Institute of Science and Technology (UNIST), Ulsan, Republic of Korea. [2]Emergent Hydrogen Technology R&D Center, Ulsan National Institute of Science and Technology (UNIST), Ulsan, Republic of Korea. [3]Department of Chemical Engineering, School of Energy and Chemical Engineering, Ulsan National Institute of Science and Technology (UNIST), Ulsan, Republic of Korea.
*These authors contributed equally to this work.
†Corresponding author. Email: jryu@unist.ac.kr (J.R.); dongwoog.lee@unist.ac.kr (D.W.L.)

RESULTS

Preparation of porous hydrogels

To enable efficient (photo)electrochemical hydrogen production, superaerophobic hydrogels were readily formed on a target electrode by cross-linking the M13 virus. This virus was chosen as the building block for the hydrogels because of its inherent nanofibrillar structure, hydrophilicity (*30*), and high stability under various conditions (*31*–*34*). At ambient temperature and pressure, the M13 virus readily forms a highly porous hydrogel through a condensation reaction with glutaraldehyde (Fig. 1A). For cross-linking, the concentration of glutaraldehyde was kept constant at 1 weight % (wt %) throughout the experiments. To improve the hydrogel's adhesion stability, the underlying substrates were modified with amine groups (see Materials and Methods); this amine modification had no effect on the (photo)electrodes' performance. To find the optimum concentration that would result in gelation, we cross-linked M13 viruses at five different concentrations: 0.1×, 0.5×, 1×, 2×, and 3× [where 1× is 5.0×10^{13} plaque-forming units (pfu) ml^{-1}]. Note that 3× is the upper concentration limit for dispersing viruses in a buffer solution without aggregations. Immediately after glutaraldehyde was added, the M13 virus solution (if it had sufficiently high concentration) was rapidly converted into a nonflowing hydrogel (Fig. 1, B and C). Next, the morphology of the cross-linked M13 virus was examined by scanning electron microscopy (SEM). At the lowest concentration (0.1×), no hydrogel was formed, as the viral solution remained as a liquid; no porous structure was observed because of insufficient cross-linking between viruses (Fig. 1D). On the contrary, at a concentration of at least 0.5×, we observed the formation of extensive cross-linked networks between the M13 viruses, resulting in gelation of the virus solutions. The measured thickness of the freeze-dried 3× hydrogel was 722 ± 201 nm (fig. S1). In the viral hydrogel, the pores' dimension and fractions were highly dependent on the concentration of the initial viral solution. In general, the increase in the concentration of the viral solution for gelation accompanied the decrease of pore size and increase of pore fraction (Fig. 1, D to I). The average pore sizes in the 0.5×, 1×, 2×, and 3× hydrogels were about 23, 21, 5, and 2 μm^2, respectively; the corresponding fractions of the pores were 17, 20, 26, and 38%, respectively.

Superaerophobicity of hydrogel-coated substrates

We hypothesized that a hydrogel's three-dimensional (3D) porous structure could provide superaerophobicity to its underlying substrate. To confirm this hypothesis, we used a captive bubble configuration to measure air-contact and air-sliding angles of Si substrates in both the absence and presence of a hydrogel overlayer (Fig. 1J and fig. S2). As expected, the hydrogel overlayer provided superaerophobicity to the underlying substrates. The air-contact angles of the pristine and 0.1×-, 0.5×-, 1×-, 2×-, and 3×-modified Si substrates were 133.3°, 148.8°, 150.6°, 153.0°, 155.8°, and 159.29°, respectively. The corresponding air-sliding angles were 12.0°, 12.0°, 2.7°, 2.0°, 2.0°, and 1.1°, respectively. The air-contact angle was higher than the baseline after treatment with even the 0.1× viral solution, suggesting that the M13 viruses were physisorbed and immobilized on the Si substrate without gelation. Although all the substrates with the cross-linked viral overlayer exhibited sufficiently high air-contact angles, only those with the viral hydrogel had a substantially lower air-sliding angle than the former. This indicates that the hydrogel-coated substrate can readily eliminate air bubbles (see the video clip in the Supplementary Materials), but the pristine and 0.1×-coated substrates cannot. These results support our hypothesis and show that the porous hydrogel overlayer—not its precursor (i.e., the M13 virus)—is responsible for the superaerophobicity. This suggests the importance of the 3D porous structure.

Effect of superaerophobic hydrogels on electrochemical hydrogen evolution reactions

We also expected that the electrochemical gas evolution reactions would exhibit stronger performance with the superaerophobic hydrogels because those hydrogels would efficiently eliminate adhered hydrogen bubbles from the electrodes' surface (Fig. 2A). To test this hypothesis, we selected Pt film as the model HER electrode/catalyst. Note that we intentionally avoid the use of nanostructured electrodes or catalysts to investigate the effect of superaerophobic hydrogels on the enhanced HER activity because nanostructure of catalyst itself can impart superaerophobicity to the catalysts (*15*). We modified the surface of Pt electrodes with cross-linked 0.1×, 0.5×, 1×, 2×, and 3× viral solution. While 0.1× led to the immobilization of the M13 virus, the rest of the cases led to gelation, after the cross-linking reactions. At first, the polarization curves were measured in 0.5 M H_2SO_4 with an iR correction. Note that the underlying substrates were treated with (3-aminopropyl) triethoxysilane (APTES) before cross-linking reactions for stable attachment of the cross-linked viral film or hydrogels via covalent bonding. The APTES treatment hardly affected the electrochemical performance of the underlying electrode (fig. S3). As shown in Fig. 2B and fig. S4, the HER onset potential—which is about 0.028 V versus a reversible hydrogen electrode (RHE)—barely differed as a result of modification with the viral overlayer. However, the HER overpotential greatly depends on the modification conditions. Although there was a negligible change in the overpotential after application of 0.1× viral film (−0.190 for the pristine one versus −0.196 V for the 0.1×-coated one at 10 mA cm^{-2}), the overpotential was considerably decreased to −0.146 V when modified with 3× viral hydrogels. In general, the HER performance of the hydrogel-modified Pt electrode increased with the porosity of the superaerophobic hydrogel (fig. S5).

To elucidate the underlying mechanism for the performance improvement, we measured electrochemical impedance spectroscopy (EIS) and double-layer capacitance of the Pt electrode and tested the HER activity of the electrode in an electrolyte solution–containing surfactant. The double-layer capacitance of the Pt electrodes, both with and without the 3× hydrogel, was measured (fig. S6) to exclude the effects of variations in the specific surface area. The double-layer capacitance was slightly lower with the deposition of the hydrogel overlayer (versus 1.55×10^{-4} mF cm^{-2}) than without it (2.02×10^{-4} mF cm^{-2}). According to EIS analysis (fig. S7), the charge transfer resistance of the Pt electrode decreased from 2.21 to 1.19 ohms at −0.15 V versus RHE after the deposition of the 3× hydrogel. In addition, there was also a decrease of the series resistance related to ionic conduction through an electrolyte and electronic conduction through an external circuit. These results suggest that the efficiencies of the charge transfer at the electrode-electrolyte interface and mass transport in an electrolyte solution were enhanced after the deposition of the superaerophobic hydrogel. To confirm that the improved performance is originating from the superaerophobicity of the hydrogel rather than improved catalytic activity of the electrodes via alteration of the binding energy and configuration of reactants/intermediates, we compared the HER performance of the corresponding Pt electrodes in an electrolyte solution–containing surfactant. In the presence of the surfactant, the amounts of hydrogen bubbles attached to the electrode were substantially reduced and there was a negligible difference

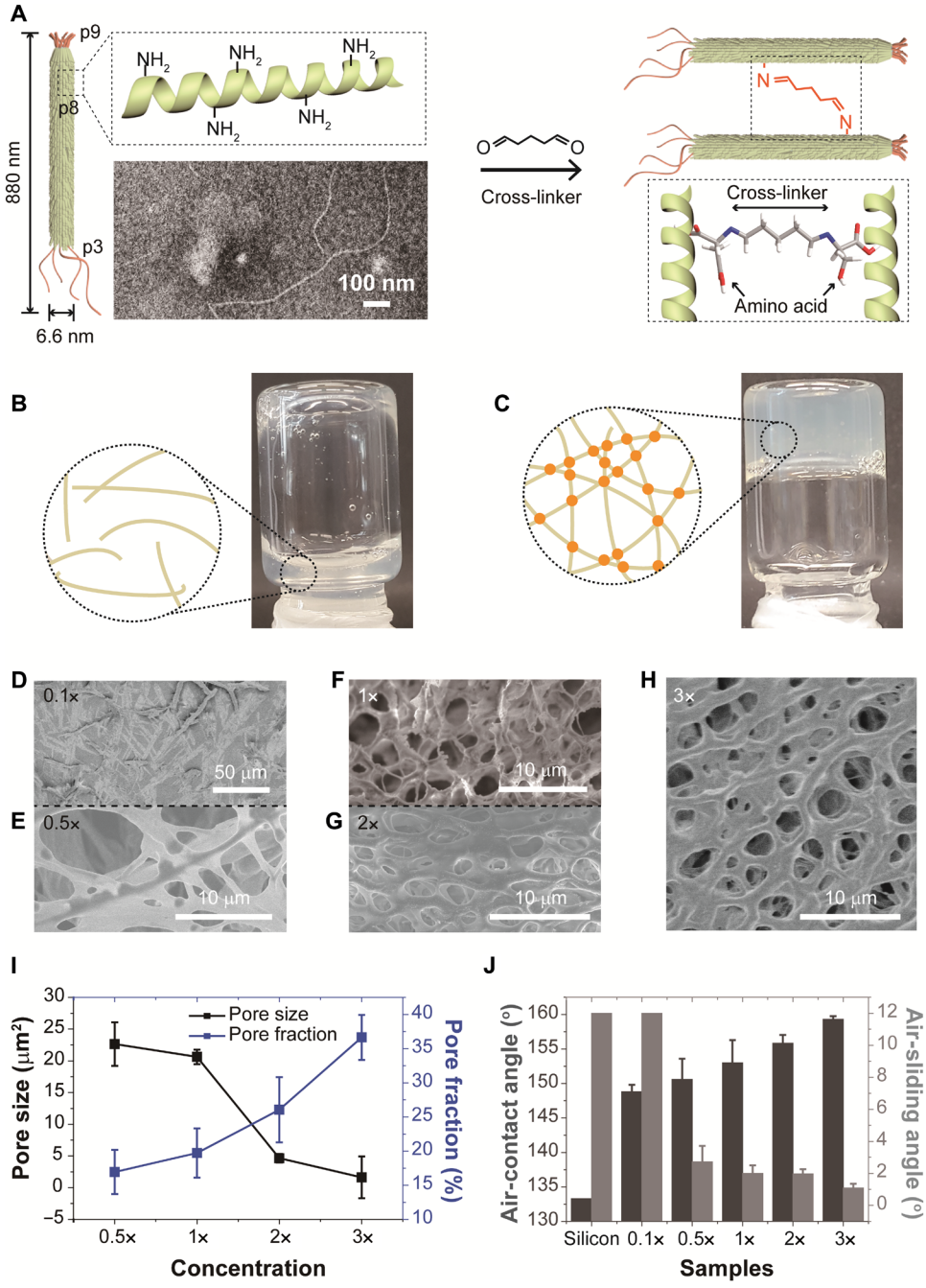

Fig. 1. Superaerophobicity of M13 viral hydrogels. (**A**) Reaction scheme for the gelation of an M13 virus solution through chemical cross-linking with glutaraldehyde. A micrograph of negatively stained M13 virus shows its nanofibrillar structure. (**B** and **C**) Photographs of the viral solutions (B) before and (C) after the gelation. Photo credit: Dasom Jeon and Jinwoo Park, Ulsan National Institute of Science and Technology. (**D** to **H**) SEM micrographs of Si substrates with a cross-linked viral overlayer: (D) 0.1× viral film and (E) 0.5×, (F) 1×, (G) 2×, and (H) 3× hydrogels. The 1× viral solution is 5.0×10^{13} pfu ml^{-1}. (**I**) Pore size and fraction of various hydrogels. (**J**) Effect of the viral hydrogel overlayer on the aerophobicity of the underlying Si substrate.

between the HER performance of the electrodes with and without the superaerophobic hydrogel (fig. S8). These results demonstrate that the efficient removal of gas bubbles by the superaerophobic hydrogel is responsible for the observed performance improvement and overwhelms the counter effect by a slight reduction of electrochemical surface area after the deposition of the superaerophobic hydrogel.

On the basis of these results, we measured chronoamperogram at various applied potentials (Fig. 2C and fig. S9). The superaerophobic hydrogel has a negligible effect at lower potentials. On the contrary, there were remarkable and bigger differences between the current densities at higher potentials where more hydrogen bubbles can be formed and attached (Fig. 2C and fig. S9). For example, the current densities of the pristine and 3× hydrogel–coated Pt electrodes

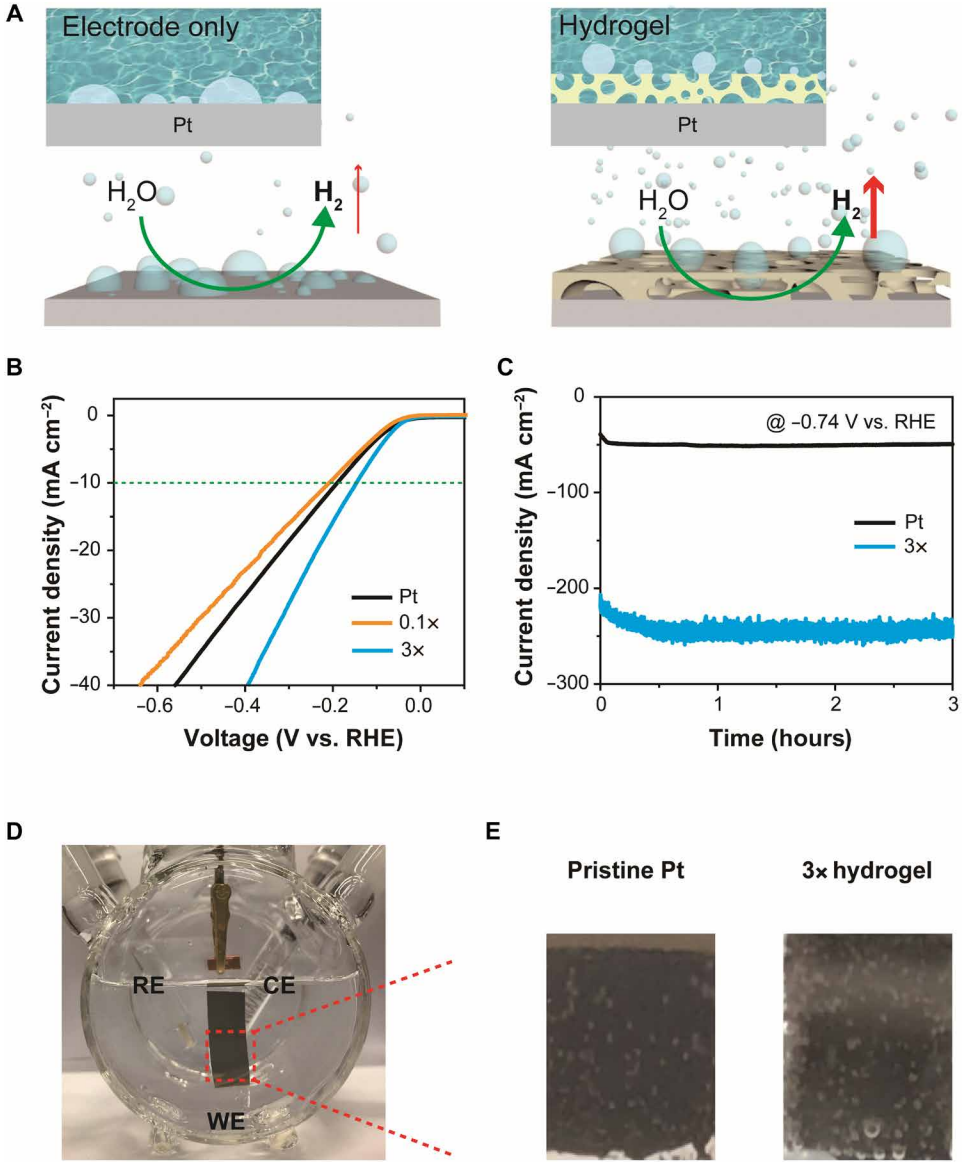

Fig. 2. Effect of the superaerophobic hydrogel overlayer on the performance of Pt electrodes in hydrogen evolution reactions (HER). (**A**) Schematic illustrations for the electrochemical HER performance of Pt electrodes with and without the superaerophobic hydrogel. (**B**) Polarization curve and (**C**) chronoamperograms of Pt electrodes before and after the modification with the cross-linked viral film (0.1×) or with the superaerophobic hydrogels (3×). The inset shows the relationship between the applied bias and the measured current densities for the corresponding electrodes. (**D** and **E**) Photographs showing (D) the experimental setup for (E) the observation of electrode surfaces during the HER. CE, counter electrode; RE, reference electrode; WE, working electrode. (D) Photo credit: Dasom Jeon and Jinwoo Park, Ulsan National Institute of Science and Technology.

were approximately −18 and −27 mA cm^{-2} at −0.3 V versus RHE and −51 and −254 mA cm^{-2} at 0.74 V, respectively (Fig. 2C). In addition, the superaerophobic hydrogel remained stable for at least 30 hours without noticeable delamination and severe performance degradation (fig. S9). SEM and Fourier transform infrared (FTIR) spectroscopy analyses (fig. S10) show that there was negligible degradation of structure and functional groups of the hydrogel after the electrochemical stability test, except for the decrease of porosity possibly due to the capillary collapse of the structure upon drying. Major peaks corresponding to C—N (1300 cm^{-1}), —CH_3 (1456 cm^{-1}), —NH_2 (1545 cm^{-1}), C═N (1652 cm^{-1}), —CH_2 (2935, 2970 cm^{-1}), and —NH_2 (3300 cm^{-1}) groups remained almost identical before and after the test.

To investigate the effect of the superaerophobic hydrogel on bubble detachment, we observed the bubble-releasing behavior (Fig. 2, D and E) by monitoring the pristine and 3× hydrogel–coated electrodes' surfaces at a constant applied potential of −0.3 V versus RHE (Fig. 2E). Contrary to our expectation, the hydrogel-coated electrode (despite having a higher performance) produced more hydrogen bubbles than the pristine one. In previous studies, researchers have reported that nano- and microstructured electrodes can exhibit superaerophobicity that enhances electrode performance by decreasing the number and size of the gas bubbles that attach to the electrode's surface (*25*–*29*). The discrepancy between this study's results and those of previous studies can be attributed to distinct strategies for

creating superaerophobic surfaces. Unlike previous studies based on nano- and microfabrication of electrodes, we deposited a 3D porous hydrogel to impart superaerophobicity to the underlying electrode. Thus, in our superaerophobic hydrogel-modified Pt, the small bubbles at the electrode-hydrogel interface can readily be transferred to the hydrogel-water interface by moving through the porous network. Meanwhile, for the bare Pt, most of the bubbles were at the electrode-water interface and grew to a certain size before detaching when the buoyancy force overwhelmed the adhesion force. The hydrogel-modified electrode, despite having more bubble than the pristine one, minimized both blocking of active sites and increase of the concentration overpotential because of the separation in the catalytically active and superaerophobic sites. Combined with the contact angle measurements (Fig. 1, G and H), these results strongly support our hypothesis that the deposition of a 3D porous hydrogel can improve HER performance by facilitating the removal of bubbles from an electrode's surface.

Enhanced photoelectrochemical hydrogen production by superaerophobic hydrogel

Our approach can also be used in photoelectrochemical systems due to the transparency of the viral hydrogel, especially in the visible light region. The density of the freeze-dried hydrogel was less than 10 mg cm^{-3}, implying that the viruses account for less than 1% of the hydrogel's overall weight. As expected from this result, the viral hydrogel was highly transparent throughout the entire visible light region (Fig. 3A). To check the validity of our approach for use in photoelectrochemical systems, we prepared p-type black Si photocathodes decorated with Pt nanoparticles (Pt/b-Si), both with and without the porous viral hydrogel overlayer; we then compared their photoelectrochemical performance under front-side (electrode-electrolyte side) visible light illumination (Fig. 3B). As in the electrochemical HER using Pt, the deposition of the hydrogel overlayer had a negligible effect on the onset potential (Fig. 3C) but substantially increased the photocurrent densities (Fig. 3, C and D). The onset potential was about 0.1 V versus RHE, regardless of the deposition of the hydrogel. Note that this relatively high onset potential can be ascribed to the formation of an insulating oxide layer. As expected, however, there was a notable increase in the photocurrent density after the deposition of the porous hydrogel; at −0.9 V versus RHE, the bare and hydrogel-coated Pt/b-Si photocathodes exhibited photocurrent densities of >22 and >15 mA cm^{-2}, respectively. These results demonstrate the versatility of our approach by showing that it can be applied to a photoelectrochemical system rather than only electrochemical one.

DISCUSSION

In terms of practical applications of our approach, the following issues should be addressed in the future. First, the validity and effectiveness of our approach should be demonstrated in more diverse

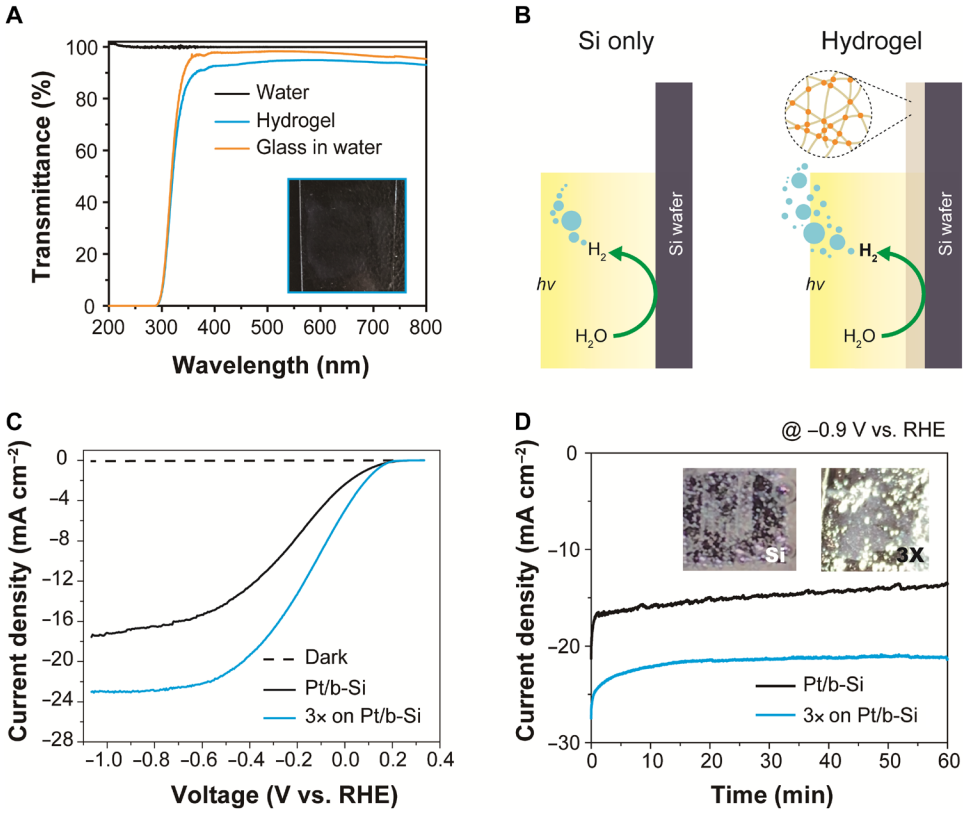

Fig. 3. Superaerophobic hydrogels for photoelectrochemical hydrogen production. (**A**) Ultraviolet-visible transmittance spectra of the slide glasses with and without the 3× hydrogel overlayer. The inset shows a photograph of the glass slide with the 3× hydrogel. (**B**) Experimental scheme, (**C**) linear sweep voltammograms, and (**D**) chronoamperograms (measured at 0–0.9 V versus RHE) showing the transparent superaerophobic hydrogel's beneficial effect on the Si photocathodes' photoelectrochemical performance for HER under front illumination with visible light (100 mW cm^{-2}). The inset images are representative photographs of the corresponding photocathodes during HER. (D) Photo credit: Dasom Jeon and Jinwoo Park, Ulsan National Institute of Science and Technology.

systems. Although we used virus-assembled hydrogels for this study's proof-of-concept demonstration, polymeric superaerophobic hydrogels should also be tested for low cost and scale-up applications. Next, considering that there is a limited number of OER catalysts efficiently and reliably working at acidic pHs (*35*, *36*), one can also check the validity of our approach in alkaline pHs. Last, it is important to demonstrate that our approach can also be effectively used on a large scale. We are currently carrying out follow-up studies to address these issues.

In summary, we developed a simple strategy for the realization of superaerophobic surfaces—particularly for gas evolution (photo) electrodes—based on the deposition of superaerophobic hydrogels on a target surface. Using M13 viral hydrogels as the model system, we found that the 3D porous structure of the viral hydrogel can impart superaerophobicity to the underlying substrate, thus readily eliminating gas bubbles. The electrodes' performance of gas evolution reactions (e.g., HER) was substantially improved as a result of the separation of catalytically active and superaerophobic sites. In addition, our approach can also be successfully applied to photoelectrodes due to the transparency of hydrogel; by contrast, conventional approaches, which rely on the nano- and microfabrication of electrodes, have lower transparency. This study can provide insight into a simple method for the design and fabrication of efficient power- and solar-to-gas conversion devices.

MATERIALS AND METHODS

Materials

Glutaraldehyde was obtained from Alfa Aesar (Ward Hill, MA, USA), and the wild-type M13 bacteriophage was purchased from New England Biolabs (Ipswich, MA, USA). All chemicals, unless stated otherwise, were purchased from Sigma-Aldrich (St. Louis, MO, USA).

Deposition of viral hydrogels

Before the deposition of the viral hydrogels, all substrates were immersed in a 10% (v/v) solution of APTES in absolute ethanol for 10 min, rinsed with absolute ethanol, dried with N_2, and baked at 125°C for 30 min (*37*). The M13 viral solutions were prepared at five different concentrations: 0.1×, 0.5×, 1×, 2×, and 3× (where 1× is 5.0×10^{13} pfu ml^{-1}). For the deposition of the hydrogel, a drop of an M13 virus solution was placed on the desired substrate, uniformly spread using doctor-blading technique, and cross-linked using 1% (w/w) glutaraldehyde.

Characterizations

Morphology of substrates was observed with an S-4800 scanning electron microscope (Hitachi High-Technologies, Japan). Hydrogel-coated substrates were freeze-dried before observing their morphology. Average pore size and fraction of viral hydrogels were calculated using ImageJ freeware (https://imagej.nih.gov/ij/). The air-contact and air-sliding angles were measured using a DSA100 drop shape analyzer (KRÜSS GmbH, Germany). Then, the ultraviolet-visible transmittance spectra of the samples were collected using a V-730 spectrophotometer (Jasco, Japan). FTIR spectroscopy analysis was performed with a 670/620 spectrometer (Agilent, USA).

Electrochemical characterizations

All (photo)electrochemical characterizations were conducted in 0.5 M H_2SO_4. The planar Pt electrodes were prepared by depositing a 100-nm Pt film on fluorine-doped tin oxide (FTO) substrates using e-beam evaporation. The black Si photocathodes (b-Si) were prepared according to the literature (*38*, *39*). The b-Si samples were firstly immersed in 0.4 M hydrogen fluoride (HF) solution for 3 min. After that, Pt nanoparticles were deposited by immersion of the b-Si samples into 0.4 M HF solution and K_2PtCl_6 for 9 min (*40*). Polarization curves were measured in the absence and presence of the cross-linked viral overlayer using an SP-150 potentiostat/galvanostat (Bio-Logic Science Instruments, France) under the following conditions: a reference electrode, Ag/AgCl; a counter electrode, FTO coated with 100-nm-thick Pt; and scan rate, 5 mV s^{-1}. Electrochemical impedance spectra were measured under the following conditions: a reference electrode, Ag/AgCl; a counter electrode, FTO-coated with 100-nm-thick Pt; applied potential, −0.15 V versus RHE; amplitude, 20 mV; and frequency scan range, 100 kHz to 0.1 Hz. For the photoelectrochemical measurements, a 300-W Xe lamp (Newport Corp., Irvine, CA, USA) equipped with a 400-nm cut-on filter (100 mW cm^{-2}) was used as a light source.

SUPPLEMENTARY MATERIALS

Supplementary material for this article is available at http://advances.sciencemag.org/cgi/content/full/6/15/eaaz3944/DC1

REFERENCES AND NOTES

1. J. Hu, C. Zhang, L. Jiang, H. Lin, Y. An, D. Zhou, M. K. H. Leung, S. Yang, Nanohybridization of MoS_2 with layered double hydroxides efficiently synergizes the hydrogen evolution in alkaline media. *Joule* **1**, 383–393 (2017).
2. S. M. Thalluri, B. Wei, K. Welter, R. Thomas, V. Smirnov, L. Qiao, Z. Wang, F. Finger, L. Liu, Inverted pyramid textured p-silicon covered with Co_2P as an efficient and stable solar hydrogen evolution photocathode. *ACS Energy Lett.* **4**, 1755–1762 (2019).
3. Z.-p. Xiang, H.-q. Deng, P. Peljo, Z.-y. Fu, S.-l. Wang, D. Mandler, G.-q. Sun, Z.-x. Liang, Electrochemical dynamics of a single platinum nanoparticle collision event for the hydrogen evolution reaction. *Angew. Chem. Int. Ed.* **57**, 3464–3468 (2018).
4. F. Sun, G. Wang, Y. Ding, C. Wang, B. Yuan, Y. Lin, NiFe-based metal–organic framework nanosheets directly supported on nickel foam acting as robust electrodes for electrochemical oxygen evolution reaction. *Adv. Energy Mater.* **8**, 1800584–1800594 (2018).
5. Y. Lin, Z. Tian, L. Zhang, J. Ma, Z. Jiang, B. J. Deibert, R. Ge, L. Chen, Chromium-ruthenium oxide solid solution electrocatalyst for highly efficient oxygen evolution reaction in acidic media. *Nat. Commun.* **10**, 162–174 (2019).
6. X. F. Lu, L. Yu, J. Zhang, X. W. Lou, Ultrafine dual-phased carbide nanocrystals confined in porous nitrogen-doped carbon dodecahedrons for efficient hydrogen evolution reaction. *Adv. Mater.* **31**, 1900699–1900706 (2019).
7. Y. Chen, G. Yu, W. Chen, Y. Liu, G.-D. Li, P. Zhu, Q. Tao, Q. Li, J. Liu, X. Shen, H. Li, X. Huang, D. Wang, T. Asefa, X. Zou, Highly active, nonprecious electrocatalyst comprising borophene subunits for the hydrogen evolution reaction. *J. Am. Chem. Soc.* **139**, 12370–12373 (2017).
8. D. Gao, R. M. Arán-Ais, H. S. Jeon, B. Roldan Cuenya, Rational catalyst and electrolyte design for CO_2 electroreduction towards multicarbon products. *Nat. Catal.* **2**, 198–210 (2019).
9. E. Liu, J. Li, L. Jiao, H. T. T. Doan, Z. Liu, Z. Zhao, Y. Huang, K. M. Abraham, S. Mukerjee, Q. Jia, Unifying the hydrogen evolution and oxidation reactions kinetics in base by identifying the catalytic roles of hydroxyl-water-cation adducts. *J. Am. Chem. Soc.* **141**, 3232–3239 (2019).
10. M. Nazemi, S. R. Panikkanvalappil, M. A. El-Sayed, Enhancing the rate of electrochemical nitrogen reduction reaction for ammonia synthesis under ambient conditions using hollow gold nanocages. *Nano Energy* **49**, 316–323 (2018).
11. J.-H. Zhou, Y.-W. Zhang, Metal-based heterogeneous electrocatalysts for reduction of carbon dioxide and nitrogen: Mechanisms, recent advances and perspective. *Reaction Chem. Eng.* **3**, 591–625 (2018).
12. Y. Choi, D. Jeon, Y. Choi, D. Kim, N. Kim, M. Gu, S. Bae, T. Lee, H.-W. Lee, B.-S. Kim, J. Ryu, Interface engineering of hematite with nacre-like catalytic multilayers for solar water oxidation. *ACS Nano* **13**, 467–475 (2019).
13. S. Bae, J.-E. Jang, H.-W. Lee, J. Ryu, Tailored assembly of molecular water oxidation catalysts on photoelectrodes for artificial photosynthesis. *Eur. J. Inorg. Chem.* **2019**, 2040–2057 (2019).

14. Z. Zhang, G. Liu, X. Cui, B. Chen, Y. Zhu, Y. Gong, F. Saleem, S. Xi, Y. Du, A. Borgna, Z. Lai, Q. Zhang, B. Li, Y. Zong, Y. Han, L. Gu, H. Zhang, Crystal phase and architecture engineering of lotus-thalamus-shaped Pt-Ni anisotropic superstructures for highly efficient electrochemical hydrogen evolution. *Adv. Mater.* **30**, e1801741 (2018).
15. X. Yu, Z.-Y. Yu, X.-L. Zhang, Y.-R. Zheng, Y. Duan, Q. Gao, R. Wu, B. Sun, M.-R. Gao, G. Wang, S.-H. Yu, "Superaerophobic" nickel phosphide nanoarray catalyst for efficient hydrogen evolution at ultrahigh current densities. *J. Am. Chem. Soc.* **141**, 7537–7543 (2019).
16. G. Zhang, Y.-S. Feng, W.-T. Lu, D. He, C.-Y. Wang, Y.-K. Li, X.-Y. Wang, F.-F. Cao, Enhanced catalysis of electrochemical overall water splitting in alkaline media by Fe doping in Ni_3S_2 nanosheet arrays. *ACS Catal.* **8**, 5431–5441 (2018).
17. C. Zhu, Q. Shi, S. Feng, D. Du, Y. Lin, Single-atom catalysts for electrochemical water splitting. *ACS Energy Lett.* **3**, 1713–1721 (2018).
18. C. N. R. Rao, M. Chhetri, Borocarbonitrides as metal-free catalysts for the hydrogen evolution reaction. *Adv. Mater.* **31**, 1803668 (2019).
19. Y. Han, K. Choi, H. Oh, C. Kim, D. Jeon, C. Lee, J. H. Lee, J. Ryu, Cobalt polyoxometalate-derived $CoWO_4$ oxygen-evolving catalysts for efficient electrochemical and photoelectrochemical water oxidation. *J. Catal.* **367**, 212–220 (2018).
20. Q. Yin, J. M. Tan, C. Besson, Y. V. Geletii, D. G. Musaev, A. E. Kuznetsov, Z. Luo, K. I. Hardcastle, C. L. Hill, A fast soluble carbon-free molecular water oxidation catalyst based on abundant metals. *Science* **328**, 342–345 (2010).
21. A. Sartorel, M. Carraro, G. Scorrano, R. De Zorzi, S. Geremia, N. D. McDaniel, S. Bernhard, M. Bonchio, Polyoxometalate embedding of a tetraruthenium(IV)-oxo-core by template-directed metalation of $[\gamma\text{-}SiW_{10}O_{36}]^{8-}$: A totally inorganic oxygen-evolving catalyst. *J. Am. Chem. Soc.* **130**, 5006–5007 (2008).
22. J. Wang, Y. Zheng, F.-Q. Nie, J. Zhai, L. Jiang, Air bubble bursting effect of lotus leaf. *Langmuir* **25**, 14129–14134 (2009).
23. C. Dorrer, J. Rühe, Superaerophobicity: Repellence of air bubbles from submerged, surface-engineered silicon substrates. *Langmuir* **28**, 14968–14973 (2012).
24. B. Su, Y. Tian, L. Jiang, Bioinspired interfaces with superwettability: From materials to chemistry. *J. Am. Chem. Soc.* **138**, 1727–1748 (2016).
25. Z. Lu, W. Zhu, X. Yu, H. Zhang, Y. Li, X. Sun, X. Wang, H. Wang, J. Wang, J. Luo, X. Lei, L. Jiang, Ultrahigh hydrogen evolution performance of under-water "Superaerophobic" MoS_2 nanostructured electrodes. *Adv. Mater.* **26**, 2683–2687 (2014).
26. Y. Li, H. Zhang, T. Xu, Z. Lu, X. Wu, P. Wan, X. Sun, L. Jiang, Under-water superaerophobic pine-shaped Pt nanoarray electrode for ultrahigh-performance hydrogen evolution. *Adv. Funct. Mater.* **25**, 1737–1744 (2015).
27. W. Xu, Z. Lu, P. Wan, Y. Kuang, X. Sun, High-performance water electrolysis system with double nanostructured superaerophobic electrodes. *Small* **12**, 2492–2498 (2016).
28. J. Hao, W. Yang, Z. Huang, C. Zhang, Superhydrophilic and superaerophobic copper phosphide microsheets for efficient electrocatalytic hydrogen and oxygen evolution. *Adv. Mater. Interfaces* **3**, 1600236 (2016).
29. M. Jiang, H. Wang, Y. Li, H. Zhang, G. Zhang, Z. Lu, X. Sun, L. Jiang, Superaerophobic RuO_2-based nanostructured electrode for high-performance chlorine evolution reaction. *Small* **13**, 1602240 (2017).
30. E. Alberts, C. Warner, E. Barnes, K. Pilkiewicz, E. Perkins, A. Poda, Genetically tunable M13 phage films utilizing evaporating droplets. *Colloids Surf. B Biointerfaces* **161**, 210–218 (2018).
31. S. D. Branston, E. C. Stanley, J. M. Ward, E. Keshavarz-Moore, Determination of the survival of bacteriophage M13 from chemical and physical challenges to assist in its sustainable bioprocessing. *Biotechnol. Bioprocess Eng.* **18**, 560–566 (2013).
32. A. Hernández-Gordillo, A. Campero, L. I. Vera-Robles, Mesoporous TiO_2 synthesis using a semi-hard biological template. *Microporous Mesoporous Mater.* **270**, 140–148 (2018).
33. J. L. González-Cansino, M. T. Vieyra-Eusebio, L. I. Vera-Robles, A. Hernández-Arana, Environmental adjustments of the cooperativity in M13 phage thermal denaturation. *Thermochim. Acta* **672**, 53–59 (2019).
34. C. Lim, J. Ko, D. Jeon, Y. Song, J. Park, J. Ryu, D. W. Lee, Probing molecular mechanisms of M13 bacteriophage adhesion. *Commun. Chem.* **2**, 96 (2019).
35. S. K. Cho, J. Chang, Electrochemically identified ultrathin water-oxidation catalyst in neutral pH solution containing Ni^{2+} and its combination with photoelectrode. *ACS Omega* **2**, 432–442 (2017).
36. D. Weber, L. M. Schoop, D. Wurmbrand, S. Laha, F. Podjaski, V. Duppel, K. Müller, U. Starke, B. V. Lotsch, IrOOH nanosheets as acid stable electrocatalysts for the oxygen evolution reaction. *J. Mater. Chem. A* **6**, 21558–21566 (2018).
37. N. K. Mani, S. Rudiuk, D. Baigl, Spatially controlled DNA unzipping by microfluidic interface positioning on a molecule perpendicular to a multicomponent flow. *Chem. Commun.* **49**, 6858–6860 (2013).
38. Y. Zhao, N. C. Anderson, M. W. Ratzloff, D. W. Mulder, K. Zhu, J. A. Turner, N. R. Neale, P. W. King, H. M. Branz, Proton reduction using a hydrogenase-modified nanoporous black silicon photoelectrode. *ACS Appl. Mater. Interfaces* **8**, 14481–14487 (2016).
39. Y. Zhao, N. C. Anderson, K. Zhu, J. A. Aguiar, J. A. Seabold, J. van de Lagemaat, H. M. Branz, N. R. Neale, J. Oh, Oxidatively stable nanoporous silicon photocathodes with enhanced onset voltage for photoelectrochemical proton reduction. *Nano Lett.* **15**, 2517–2525 (2015).
40. I. Oh, J. Kye, S. Hwang, Enhanced photoelectrochemical hydrogen production from silicon nanowire array photocathode. *Nano Lett.* **12**, 298–302 (2012).

Acknowledgments

Funding: This work was supported by the Basic Science Research Program (2018R1D1A1A02046918 and 2019R1A2C2005854) and the Technology Development Program to Solve Climate Changes (2019M1A2A2065616) through the National Research Foundation of Korea (NRF) funded by the Ministry of Science and ICT of Korea. **Author contributions:** D.W.L. and J.R. conceived and supervised the project. D.J. and J.P. principally performed experiments and analyzed results. C.S., H.K., and J.-W.J. supported photoelectrochemical experiments. D.J., J.P., D.W.L., and J.R. wrote the manuscript. All authors read, revised, and approved the manuscript. **Competing interests:** The authors declare that they have no competing interests. **Data and materials availability:** All data needed to evaluate the conclusions in the paper are present in the paper and/or the Supplementary Materials. Additional data related to this paper may be requested from the authors.

Submitted 5 September 2019
Accepted 13 January 2020
Published 10 April 2020
10.1126/sciadv.aaz3944

Citation: D. Jeon, J. Park, C. Shin, H. Kim, J.-W. Jang, D. W. Lee, J. Ryu, Superaerophobic hydrogels for enhanced electrochemical and photoelectrochemical hydrogen production. *Sci. Adv.* **6**, eaaz3944 (2020).

Superaerophobic hydrogels for enhanced electrochemical and photoelectrochemical hydrogen production

Dasom Jeon, Jinwoo Park, Changhwan Shin, Hyunwoo Kim, Ji-Wook Jang, Dong Woog Lee and Jungki Ryu

Sci Adv **6** (15), eaaz3944.
DOI: 10.1126/sciadv.aaz3944